4,4'-Dipyridyl dioxide·SbF_3 Co-crystal: Pnictogen Bond Prevails over Halogen and Hydrogen Bonds in Driving Self-assembly

Patrick Scilabra,[†] Giancarlo Terraneo,[†] Andrea Daolio,[†] Alberto Baggioli,[†] Antonino Famulari,[†] Cesar Leroy,[‡] David L. Bryce,[‡] Giuseppe Resnati[†]*

[†] Department of Chemistry, Materials, and Chemical Engineering "Giulio Natta", Politecnico di Milano, via Mancinelli 7, 20131 Milano, Italy

[‡] Department of Chemistry and Biomolecular Sciences, University of Ottawa, 10 Marie Curie Private, Ottawa, Ontario, Canada K1N 6N5

Supporting Information

ABSTRACT: The SbF_3·4,4′-dipyridyl *N*,*N*′-dioxide co-crystal is prepared and characterized *via* infrared spectroscopy and ^{121}Sb and ^{123}Sb nuclear quadrupolar resonance. Single crystal X-ray analyses proves that a major role in co-crystal formation is played by Sb···O pnictogen bonds, the attractive interactions wherein antimony and oxygen act as the electrophilic and nucleophilic sites, respectively. Molecular Electrostatic Potential and Natural Bond Orbital analyses confirm the relevance of this interaction in the self-assembly process. Dipyridyl dioxide forms also hydrogen bonded and halogen bonded co-crystal, e.g., when water and 1,4-diiodo-tetrafluoro-benzene function as acceptors of electron density. Experiments of competitive co-crystal formation indicate that under the adopted conditions pnictogen bond prevails over halogen bond and hydrogen bond in identifying the tecton involved in co-crystal formation with dipyridyl dioxide.

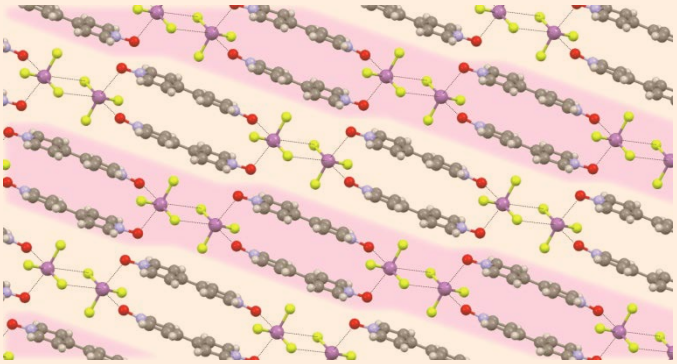

1. INTRODUCTION

Non-covalent interactions are a hot topic in supramolecular chemistry[1] thanks to the relevance they have in numerous fields spanning crystal engineering,[2] the design of molecular materials,[3] the recognition processes between small molecules and biological receptors.[4] The need to finely tune these phenomena and to control and engineer aggregation and self-assembly processes, has raised the attention on less established interactions, e.g. cation-π and anion-π bondings,[5,6] aurophilic interactions,[7] π-hole and σ-hole bondings.[8,9]

These latter interactions encompass a wide set of bondings wherein an electron rich moiety (nucleophilic site, e.g., a lone pair possessing atom or an anion, such as the nitrogen of an amine or a pyridine derivative, the oxygen of a carbonyl or an ether, a bromide or an iodide ion, the oxygen of a perchlorate or periodate ion) forms a short[10] and net attractive contact with the region of depleted electron density (σ-hole)[11] on an atom. The halogen bond (HaB),[12] and the chalcogen bond (ChB)[13] are the interactions wherein an halogen and a chalcogen atom function as the electrophilic site, respectively, and are the better known cases of the group of attractive interactions encompassed by the term σ-hole bondings. Also elements of groups 13, 14, and 15 of the periodic table can work as electrophiles and form short contacts at their positive σ-hole(s) with electron rich moieties. Consistent with the tendency to name interactions referring to the electrophilic site,[14] these contacts are typically named triel bond (TrB), tetrel bond (TtB)[15,16] and pnictogen bond (PnB).[17,18]

σ-Hole interactions present several common features, independent from the group of the periodic table to which the electrophilic atom belongs.[8,9,19] In general, interaction strength and positive electrostatic potential at the σ-hole run parallel. An atom forming n covalent bonds can have on its surface up to n positive σ-holes which can be involved in up to n net attractive interactions with electron rich sites in surrounding molecular entities. The strength of the interaction of a donor of electron density with an electrophilic element of a given group of the periodic table increases with the polarizability of the element and decreases when its electronegativity increases. For instance, fluorine, oxygen, or nitrogen typically form very weak HaBs, ChBs, and PnBs, if any, while interactions formed by iodine, tellurium, or antimony are fairly strong. For a given element, the more electron withdrawing a covalently bonded residue, the greater the depletion of electron density at the σ-hole opposite the covalent bond it forms.[8,9,16] For instance, σ-holes opposite to a fluorine or cyano group are more extended and their surface electrostatic potential more positive than σ-holes associated with most other substituents.

σ-Hole interactions typically occur on the elongation of the covalent bond responsible for the hole formation and this directionality is another common and distinctive feature.[8,9] This preferential linearity is related to the σ-hole

localization on atom surface and may offer additional advantages in crystal engineering and recognition processes.[20] Experimental evidences[17,18,21] show that ChBs and even more PnBs frequently present greater deviations from linearity than HaB and TtB. Theoretical calculations[9,22] reveal that this corresponds to a dislocation of the σ-hole from the extension of the covalent bond, a likely consequence of the anisotropic electronic effects of the substituents at the chalcogen and pnictogen atoms and the presence of lone pair(s) on these atoms.

Several theoretical studies[23] and some Cambridge Structural Database surveys[17,18] suggested a remarkable ability of PnB to affect self-assembly processes, but designed and experimental confirmations of this ability are less numerous.[19,24,25] In order to test of ability of PnB to drive the formation of co-crystals, we studied the aggregation features of antimony(III) fluoride, a commonly used fluorinating reagent in organic chemistry (Swarts reagent) and, expectedly, a strong PnB donor. It has been reported[26] that SbF_3 has three remarkably positive σ-holes, consistent with the high polarizability of antimony and high electronegativity of fluorine. We report here the formation of the SbF_3·4,4′-dipyridyl *N*,*N*′-dioxide co-crystal (**1**) (Figure 1), its characterization *via* single crystal X-ray analyses and nuclear quadrupole resonance (NQR) analyses, as well as some computational results on derivatives where pnictogen atoms bear fluorine and cyano substituents. Dipyridyl dioxide has a remarkable tendency to form hydrogen bonded co-crystals, the solvate with water can be considered the prototype of such adducts.[27] In the presence of a HaB donor as good as 1,4-diiodotetrefluorobenzene, formation of halogen bonded co-crystals if favored over the formation of hydrogen bonded co-crystals.[28] Competitive co-crystallization experiments showed that SbF_3 is a PnB donor good enough to prevail over diiodotetrafluorobenzene and water in accepting electron density from dipyridyl dioxide oxygen atoms and PnB prevails over HaB and hydrogen bond (HB) in driving co-crystal formation.

2. RESULTS AND DISCUSSION

The melting point of SbF_3 is quite high (292 °C) and is much higher than the melting point of heavier antimony trihalides (mps of $SbCl_3$, $SbBr_3$, and SbI_3 are 73, 97, and 170 °C in the order). This suggests a particularly strong propensity of the compound to be involved in intramolecular attractive interactions. Both SbF_3 and $SbCl_3$ exist in the solid phase as molecular crystals. In the overall packing of $SbCl_3$,[29] three short covalent Sb−Cl bonds (2.35−2.38 Å) form the $SbCl_3$ molecule and the shortest non-covalent Sb···Cl separation is ~350 pm, this value corresponding to a normalized contact N_c[30] ~0.92. Differently, in the packing of SbF_3,[31] SbF_3 molecules are assembled *via* three short covalent Sb–F bonds (190-194 pm) and are connected into a three dimensional network via three Sb F interactions 260-263 pm long, corresponding to Nc ~0.74. These interactions are well below the sum of van der Waals radii of Sb and F (the corresponding N_c value is ~0.74), develop approximately along the axis of the Sb–F covalent bonds, and can be considered fairly short PnBs.

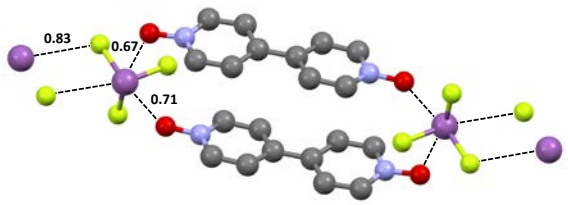

Figure 1. Ball and stick representation (Mercury 4.1.2) of a part of co-crystal **1**. Hydrogen atoms have been omitted for sake of clarity, PnBs are black dashed lines. N_c values are reported close to the interactions. Color codes: gray, carbon; light blue, nitrogen; red, oxygen; green, fluorine, violet, antimony.

Single crystal X-ray analyses. We expected that the robust network of intermolecular PnBs present in pure and crystalline SbF_3 is more likely overcome by interactions with a co-crystal former if a strong donor of electron density is used. Indeed, Cambridge structural database (CSD) analyses indicate that SbF_3 affords co-crystals typically when strong and polydentate donors of electron density (PnB acceptors) are used (e.g., anions, crown ethers, diphosphine-dioxides, see ESI).

In the attempt to obtain a co-crystal, we thus used 4,4′-dipyridyl *N*,*N*′-dioxide as PnB acceptor. 1:1 Solutions of dipyridyl dioxide and SbF_3 afforded, under different conditions, a white crystalline precipitate. IR spectrum of this white crystalline precipitate showed, with respect to pure starting compounds, non minor shifts and intensity changes for absorptions of both the dioxide and the trifluoride, consistent with the formation of a well-defined chemical species rather than a physical mixture. DSC analyses confirmed this indication as a single endothermic phenomenon, different from melting point of starting compounds, was obtained. Elongated block plates were formed when a methanol solution of SbF_3 was layered over a tetrahydrofurane solution of the dioxide. Single crystal X-ray analyses confirmed that these plates consisted in the pnictogen bonded SbF_3·4,4′-dipyridyl *N*,*N*′-dioxide co-crystal (**1**) and afforded the structural details of the self-assembled architecture (Figure 1). The homogeneity of different batches was proven by the match between the experimental patterns from powder X-ray diffraction analyses and the diffraction pattern simulated from single crystal analyses.

HBs (between the hydrogen atoms of dipyridyl units and the fluorine atoms of SbF_3 units) and PnBs (between the antimony atom of a SbF_3 unit and oxygen and fluorine atoms of closeby dipyridyl and SbF_3 units) are the closest interactions in the crystal packing of **1**. The shortest HB is characterized by an N_c value of 0.88, namely much greater than Nc values of PnBs (*vide infra*) and the following discussion will focus on the latter interactions. Two dipyridyl dioxide units double bridge two SbF_3 units and a pnictogen bonded non-covalent tetramer is assembled around an inversion center *via* four Sb···O PnBs which are

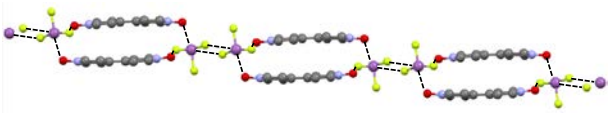

Figure 2. Ball and stick representation of the ribbon formed by the Sn─F···F PnBs (black dashed lines). Hydrogen atoms have been omitted for sake of clarity. Color codes as in Figure 1.

241.8 and 257.1 pm long (corresponding N_c values are 0.67 and 0.71). Reminiscent of what occurs in pure SbF_3, the PnB donor ability of two adjacent antimony atoms are saturated by the formation of two symmetry related Sb···F PnBs (298.4 pm, N_c=0.83) involving the regions of expected higher electron density of fluorine atoms. These PnBs connect the non-covalent tetramers mentioned above into linear ribbons (Figure 2).

Longer and weaker σ-hole interactions tend to be less linear than shorter and stronger ones,[17,20] consistent with the fact they generate milder driving forces towards formation along the axis of the covalent bond producing the hole. F–Sb···O angles are 168.41° and 164.08° (the considered F atoms are those roughly opposite the oxygen atom). These values match with the F–Sb···σ-hole angle computed in this manuscript for SbF_3 (165°, see onwards) and the angle already reported in the literature.[9] The Sb···F PnB is substantially longer, and weaker (see onwards), than Sb···O PnBs, the F–Sb···F angle being 153.52°. The non-complete substitution, on co-crystal formation, of

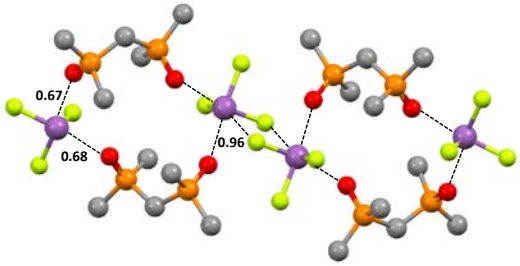

Figure 3. Ball and Stick representation of the repeating unit in the crystal packing of the antimony trifluoride·bis(dimethyl-phosphinoyl)methane adduct (Refcode UROYUW). Color codes: Orange, phosphorus; other colors as Figure 1.

Sb···O PnBs involving the co-crystal former for the Sb···F PnBs present in pure SbF_3 is quite common. This persistence of Sb···F PnBs is a further confirmation of the strength of latter interactions and of the tendency of SbF_3 to function as tridentate PnB donor. The involvement of antimony in the formation of two shorter PnBs with the co-crystal former and one longer with another SbF_3 unit has been observed in various adducts wherein the donor of electron density is an oxygen atom of a highly nucleophilic moiety (Figure 3).

NQR analyses. Nuclear magnetic resonance (NMR) and NQR are powerful tools to study σ-hole interactions. For instance, HaB formation affects chemical shifts of ^{19}F[32] and ^{13}C[33] NMR nuclei of the acceptor moiety in solution and in the solid. The same and other spectral parameters of

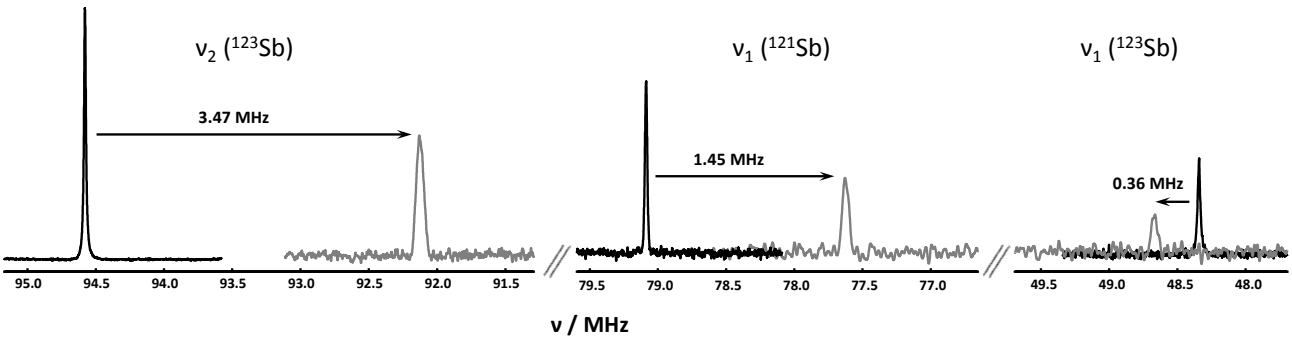

Figure 4. ^{121}Sb and ^{123}Sb Frequencies and their shifts for SbF_3·4,4'-dipyridyl dioxide adduct **1** (black) and SbF_3 (grey).

Table 1. NQR frequencies for SbF_3 and SbF_3·4,4'-dipyridyl dioxide adduct **1**. Asterisk values are calculated from experimentally observed frequencies.

ν / MHz	^{121}Sb		^{123}Sb			Experimental		
	ν_1	ν_2	ν_1	ν_2	ν_3	η_Q	$C_Q(^{121}Sb)$	$C_Q(^{123}Sb)$
SbF_3	79.08	157.62*	48.34	95.58	143.53*	0.05	525.818	670.102
SbF_3·4,4'-dipyridyl dioxide	77.63	152.43*	48.70	92.11	139.05*	0.12	509.966	649.901

^{15}N,[34] $^{35/37}$Cl,[35] ^{127}I,[36] ^{31}P,[37] ^{17}O,[38] and ^{39}Se[39] nuclei have been reported to undergo significant modifications on HaB and ChB formation.Tthe usefulness of $^{121/123}$Sb NQR spectroscopy for probing PnBs in adducts formed by SbF_3 and $SbCl_3$ was reported.[24] Experiments carried out on co-crystal **1** showed substantial changes of spectral parameters relative to pure SbF_3 (Figure 4, Table 1). The quadrupolar coupling constants of **1** for ^{121}Sb and ^{123}Sb are 509.97 and 649.90 MHz, respectively, consistent with previous observations[24] that stronger and more directional PnBs at antimony are associated with smaller C_Q values. It is also worth noting that the C_Q values for **1** are comparable to those reported for the SbF_3·urea co-crystal which has a chemical environment around the antimony atom somewhat similar to **1** as, in both adducts, the oxygen atom of two nearby electron density donor molecules engage in PnB formation.

Computational details. In order to have theoretical confirmation that deviation from linearity in PnBs and in related σ-hole interactions is also a consequence of inherent molecular features rather than an exclusive effect of crystal packing requirements, the molecular electrostatic potential (MEP) on the 0.001 a.u. electron density isosurface was calculated for some Y–X_n derivatives (Y=P, As, Sb, n=3; Y=S, Se, Te, n=2; Y=Cl, Br, I, n=1; X=F, CN). A graphic representation of the maximum values of the positive electrostatic potential ($V_{S,max}$) at Y in Y–X_n is given in Figure 5 along with the angular position θ of $V_{S,max}$ with respect to the Y–X covalent bond (Figure 6). Relativistic effects for heavy elements have been taken into account by using convenient core potentials (ECP10MDF and ECP28MDF on fourth and fifth row elements, respectively).

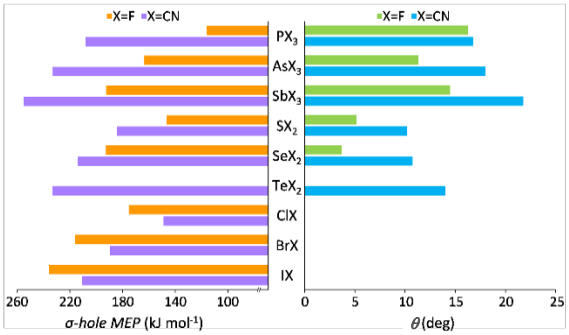

Figure 5. Histograms showing values of 0.001 a.u. $V_{S,max}$ (left) and values of angular deviations θ (right) of $V_{S,max}$ from the axis of the Y–X covalent bond associated with σ-holes in some fluorides and cyanides of groups 15-17 elements (angular deviation for halogens derivatives are not sketched since, due to symmetry, are zero for isolated molecules). Numerical values are reported in Table S3.

Figure 6. Schematic representation of angular deviation θ of $V_{S,max}$ (orange circle) from the axis of Y–X covalent bond. θ Angles for pnictogen and chalcogen derivatives (left and right) lie on a σ_v bisecting plane and on the molecular plane, respectively.

Obtained results (ESI) parallel those already available in the literature.[9] It is confirmed that the σ-hole of an element of a given group of the periodic table becomes more positive when the polarizability of the element increases. Moving from pnictogens to halogens, σ-holes generated by cyano substituents get more and more positive compared to those produced by fluorine substituents. As a result, electrostatic potential values at σ-holes on phosphorus, arsenic, and antimony tricyanides are 79%, 42%, and 32% more positive than in the corresponding trifluorides. Consistent with the anisotropic electrostatic effects determined by substituents and lone pair(s) at pnictogen and chalcogen atoms, the σ-hole position on group 15 and 16 atoms deviates from the axis of the Pn/Ch–substituent covalent bond. The deviation from linearity is larger for pnictogens than for chalcogens and the cyano group prompts larger angular deviations than fluorine group (it is as high as 22° for $Sb(CN)_3$). For cyano derivatives, deviation increases with the polarizability of group 15 and 16 element.

While the electrostatic effects usually play an important role in determining the attractive nature of σ-hole interactions and causing interpenetration of van der Waals volumes,[9] charge-transfer, polarization, and dispersion contributions are all influential[40] and their relative relevance depends on the donor, the acceptor, and the conditions in which the adducts are formed. After considering the electrostatic point of view by calculating the electron density isosurfaces, we tackled the charge-transfer perspective by performing natural bond orbital (NBO) analysis with the specific aim to have some insight into the energetic features of PnBs and the relation of these features to the interaction geometry.[41,42] Second-order perturbation theory analysis of the Fock matrix in the NBO base offers the stabilization energy term $E^{(2)}$ as a useful tool which is associated with the exchange of electron density from a Lewis-like occupied NBO to a non-Lewis-like unoccupied NBO. The relative position of nucleophilic atom Z (Z=O, F) with respect to SbF_3 was characterized by the φ angle formed by Sb---σ-hole axis and the axis of the closest Z···Sb PnB (the orientation of φ angle about the Sb---σ-hole axis was neglected here due to the relative homogeneity of the electrostatic potential gradient around the σ-hole, and the delocalized electron density around Z nucleus). $E^{(2)}$ energies and φ angles for interactions in **1** and other structurally similar adducts are reported in Table 2. It is interesting to observe that the $E^{(2)}$ energy for the Sb···O PnBs in SbF_3·(4-methoxy-pyridine *N*-oxide)$_2$ adduct **3**[43] is as high as ~103 kJ·mol^{-1}. Consistent with the established greater tendency of oxygen to act as donor of electron density than of fluorine, Sb···O PnBs in **1** are stronger than Sb···F PnB (up to ~75 kJ·mol^{-1} *vs.* ~6 kJ·mol^{-1}) and a similar relative strength of Sb···O and Sb···F interactions is found for the analogous adduct

Table 2. $E^{(2)}$ energies for PnBs in compounds **1**-**3** as obtained from NBO second-order perturbation analysis. Deviation angles φ and N_c values are also reported.

Compound	Interaction	$E^{(2)}$ (kJ/mol)	φ (°)	N_c
1	F–Sb···O	56.2	9.9	0.69
1	F–Sb···O	75.2	7.8	0.73
1	F–Sb···F	6.3	13.6	0.81
2	F–Sb···O	69.9	3.5	0.68
2	F–Sb···O	29.5	9.6	0.78
2	F–Sb···F	4.5	19.5	0.93
3	F–Sb···O	102.8	5.4	0.64

SbF_3·(pyridine *N*-oxide)$_2$ **2**[44]. As typical for σ-hole interactions, stronger interactions are more linear (smaller φ angles) and shorter (smaller N_c values) (Table 2).

Competitive co-crystal formation. When wet methanol is layered over a tetrahydrofurane solution of 4,4'-dipyridyl *N*,*N*'-dioxide, the $(H_2O)_2$·dipyridyl dioxide co-crystal[29] is formed. When 1,4-diiodotetrafluorobenzene (1 equivalent) is present in the methanol layered over the tetrahydrofurane solution of dipyridyl dioxide, the precipitation of the 1:1 diiodotetrafluorobenzene·dipyridyl dioxide co-crystal[28] is preferred over the water containing co-crystal. When *p*-diiodotetrafluorobenzene and antimony trifluoride (1 equivalent each) are present in the methanol layered over the tetrahydrofurane solution of the dipyridyl dioxide, the SbF_3·dipyridyl dioxide co-crystal **1** is formed. Under the adopted conditions, PnB is the interaction driving the co-crystal formation, namely it prevails over HaB and HB in identifying the module to be involved in the solid self-assembled system with dipyridyl dioxiide.

3. CONCLUSIONS

While computational studies[9,20,23] and CSD analyses[18] give consistent and forceful indications that PnB can work as a robust interaction to obtain co-crystals by design, very few cases have been reported where this potential has been explored.[24] The obtainment of the SbF_3·dipyridyl dioxide co-crystal **1** reported here suggests that PnB might indeed feature as a new and powerful tool in crystal engineering. Single crystal X-ray analyses of **1** affords the structural details of the self-assembled architecture. The deviation of PnBs from linearity revealed by crystallographic analyses parallels the dislocation, revealed by MEP analyses, of the σ-hole from the extension of the Sb–F covalent bonds. NBO analyses gives quite high values for stabilization energy terms $E^{(2)}$ of Sb···O PnBs. These data indicate that both the poor linearity of PnBs and the small Sb···O separations experimentally observed in the co-crystal **1** are a likely consequence of the electronic features of SbF_3 rather than a crystal packing effect.

In conclusion, results reported here increase the understanding of some key features of PnBs and may be useful in the design and realization of many other PnB driven recognition and self-assembly processes.

4. EXPERIMENTAL DETAILS

X-ray crystallography data acquisition. X-ray diffraction data were collected using a Bruker APEX-II diffractometer equipped with sealed-tube and CCD detector, and employing Mo-Kα radiation (λ=0.71073 Å). The crystals were collected using Bruker KRYOFLEX device. Semi-empirical absorption corrections and scaling were performed on datasets, exploiting multiple measures of symmetry-related reflections, using SADABS program.[45]. The structures were solved by ShelxS[46] and the refinements were carried out by full-matrix least-squares on F2 using the SHELXL program.[47] Pictures were prepared using CCDC Mercury.[48] Essential crystal and refinement data are reported in ESI.

Synthesis of SbF_3·4,4′-dipyridyl *N*,*N*′-dioxide co-crystal (1). A methanolic solution of SbF_3 was layered on top of a THF solution containing an equimolar amount 4,4′-dipyridyl *N*,*N*′-dioxide inside a clear borosilicate glass vial at room temperature. Good quality, colorless crystals with elongated block shape were obtained (mp 263 °C) in 24 hours by letting the layered solutions diffuse in the closed vial. They were suitable for single crystal X-ray diffraction.

Technical details for calculations. Calculations were carried out using the B3LYP functional as it is implemented in Gaussian16.[49] Small-core fully relativistic effective core potentials were used on fourth and fifth row elements (ECP10MDF and ECP28MDF, respectively) along with the associated triple-ζ basis sets[50-53] while correlation-consistent cc-pVTZ bases were used for lighter atoms.[54,55] Before processing chemical structures extracted from the Cambridge Structural Database (CSD), the position of any hydrogen atom was optimized at the same level while keeping the position of heavier atoms fixed. Natural bond orbital (NBO) analyses were performed using the Gaussian-embedded NBO3.1 code.[56]

NQR spectroscopy. A powdered sample of **1** was packed in a 5 mm o.d. glass tube in an argon-filled glovebox. A Bruker Avance III 400 NMR console, without applied external magnetic field, was used to record the $^{121/123}$Sb NQR spectra. A Hahn−echo pulse sequence (π/2−τ−π−τ) was used with pulse lengths of 4.6 and 9.2 μs. The recycle delay was 0.2 s. Data were collected at room temperature using a 5 mm solenoid HX probe.

■ ASSOCIATED CONTENT

The Supporting Information is available free of charge on the ACS Publication website https://pubs.acs.org/ at DOI: xxxx

■ AUTHOR INFORMATION

Corresponding Author

*E-mail: giuseppe.resnati@polimi.it

ORCID

Patrick Scilabra: 0000-0003-1972-620X
Giancarlo Terraneo: 0000-0002-1225-2577
Andrea Daolio: 0000-0003-3571-3935
Alberto Baggioli: 0000-0001-8159-6077
Antonino Famulari: 0000-0001-5287-1092
Cesar Leroy: 0000-0002-9013-5552
David L. Bryce: 0000-0002-0705-3004
Giuseppe Resnati: 0000-0002-0797-9296

Notes

The authors declare no competing financial interest.

■ REFERENCES

(1) Scheiner, S. Noncovalent Forces; Springer International Publishing, Cham, SW, **2015**.

(2) Giese, M.; Albrecht, M.; Rissanen, K. Anion-π Interactions with Fluoroarenes: *Chem. Rev.* **2015**, 115, 16, 8867-8895

(3) Priimagi, A. Cavallo G.; Metrangolo P.; Resnati G.; The Halogen Bond in the Design of Functional Supramolecular Materials: Recent Advances. *Acc. Chem. Res.* **2013**, 46, 11, 22686-2659.

(4) Newberry, R. W.; Raines, R. T. The n→ π^* Interaction. *Acc. Chem. Res.* **2017**, *50*, 1838-1846.

(5) Yamada, S.; Cation- π Interactions in Organic Synthesis. *Chem. Rev.* **2018**, *118*, 11353-11432.

(6) Frontera, A.; Gamez, P.; Mascal, M.; Mooibroek, T. J.; Reedijk, J. Putting Anion-π Interactions Into Perspective. *Angew. Chem. Int. Ed.* **2011**, *50*, 9564-9583.

(7) Schmidbaur, H.; Schier, A. Aurophilic Interactions as a Subject of current Research: an up-date. *Chem. Soc. Rev.* **2012**, 41, 370-412.

(8) Politzer, P; Murray, Jane S. An Overview of Strength and Directionalities of Noncovalent Interactions: σ-Holes and π-Holes. *Crystals*, **2019**, 9, 165.

(9) Politzer, P; Murray, J. S.; Clark, T.; Resnati, G. The σ-Hole Revisited. *Phys. Chem. Chem. Phys.* **2017**, 19, 32166-32178.

(10) Hereinafter the word short is used for non-covalent interactions where the atoms separation is smaller than the sum of van der Waals radii.

(11) Clark, T.; Hennemann, M.; Murray J. S.; Politzer, P.; Halogen Bonding: the σ-Hole. *J. Mol. Model.* **2007**, 13, 291-296.

(12) Desiraju, G. R.; Ho, P. S.; Kloo, L.; Legon, A. C.; Marquardt, R.; Metrangolo, P.; Politzer, P.; Resnati, G.; Rissanen, K.; Definition of the Halogen Bond (IUPAC Recommendations 2013). *Pure Appl. Chem.* **2013**, 85, 1711-1713.

(13) Aakeroy, C. B.; Bryce, D. L.; Desiraju, G. R.; Frontera, A.; Legon, A. C.; Nicotra, F.; Rissanen, K.; Scheiner, S.; Terraneo, G.; Metrangolo, P.; Resnati, G. Definition of the Chalcogen Bond (IUPAC Recommendations 2019). *Pure Appl. Chem.* **2019** in press. DOI: org/10.1515/pac-2018-0713.

(14) Cavallo, G.; Metrangolo, P.; Pilati, T.; Resnati, G.; Terraneo, G. Naming Interactions from the Electrophilic Site. *Cryst. Growth. Des.* **2014**, *14*, 2697-2702.

(15) Bauzà, A.; Seth, S. K.; Frontera, A.; Tetrel Bonding Interactions at Work: impact on Tin and Lead Coordination Compounds. *Coord. Chem. Rev.* **2019**, *384*, 107-125.

(16) Scilabra, P.; Kumar, V.; Ursini, M.; Resnati, G. Close Contacts Involving Germanium and Tin in Crystal Structures: Experimental Evidence of Tetrel Bonds. *J. Mol. Model.* **2018**, *24*, 37.

(17) Scilabra, P.; Terraneo, G.; Resnati, G. Fluorinated elements of Group 15 as pnictogen bond donor sites. *J. Fluorine Chem.* **2017**, *203*, 62-74.

(18) Politzer, P.; Murray, J. S.; Janjić, G. V.; Zarić, S. D. σ-Hole Interactions of Covalently-Bonded Nitrogen, Phosphorous and Arsenic: A Survey of Crystal Structures. *Crystals*, **2014**, *4*, 12-31.

(19) Benz, S, Poblador-Bahamonde, A. I.; Low-Ders, N.; Matile, S. Catalysis with Pnictogen, Chalcogen and Halogen Bonds. *Angew. Chem. Int.* **2018**, *57*, 5408-5412.

(20) Bauzà, A.; Mooibroek, T. J.; Frontera, A.; The Bright Future of Unconventional σ/π-Hole Interactions. *Phys. Chem Phys Chem.* **2015**, *16*, 2496-2517.

(21) Scilabra, P.; Terraneo, G.; Resnati, G. The Chalcogen Bond in Crystalline Solids: A World Parallel to Halogen Bond. *Acc. Chem. Res.* **2019**, *52*, 1313-1324.

(22) Adhikari, U.; Scheiner, S. Sensitivity of Pnicogen, Chalcogen, Halogen and H-Bonds to Angular Distortions. *Chem. Phys. Lett.* **2012**. *532*, 31-35.

(23) Scheiner, S. The Pnictogen Bond: Its Relation to Hydrogen, Halogen, and Other Noncovalent Bonds. *Acc. Chem. Res.* **2013**, *46*, 280-288.

(24) Trubenstein, H. J.; Moaven, S.; Vega, M.; Unruh, D. K.; Cozzolino, A. F. Pnictogen Bonding with Alkoxide Cages: Which Pnictogen is Best? *New J. Chem.* **2019**, *43*, 14305-14312.

(25) Leroy, C.; Johannson, R.; Bryce, D. L. $^{121/123}$Sb Nuclear Quadrupole Resonance Spectroscopy: Characterization of Non-Covalent Pnictogen Bonds and NQR Crystallography. *J. Phys. Chem. A*, **2019**, *123*, 1030-1043.

(26) Bauzà, A.; Mooibroek, T. J.; Frontera, A. σ-Hole Opposite to a Lone Pair: Unconventional Pnictogen Bonding Interactions between ZF_3 (Z=N, P, As, and Sb) Compounds and Several Donors. *Chem. Phys. Chem.* **2016**, *17*, 1608-1614.

(27) Thaimattam, R.; Shekhar Reddy, D.; Xue, F.; Mak, T. C. W.; Nangia, A.; Desiraju, G. R. Interplay of strong and weak hydrogen bonding in molecular complexes of some 4,4'-disubstituted biphenyls with urea, thiourea and water. *J. Chem. Soc. Pekin Trans 2* **1998**, 1783-1789.

(28) Corradi, E.; Meille S. V.; Messina, M. T.; Metrangolo, P.; Resnati, G. Halogen Bonding versus Hydrogen Bonding in Driving Self-Assembly Processes. *Angew. Chem. Int. Ed.* **2000**, *39*, 1782-1786.

(29) Lindqvist, I.; Niggli, A. The Crystal Structure of Antimony Trichloride. *J. Inorg. Nucl. Chem.* **1956**, *2*, 345-347.

(30) The "normalized contact" N_C for an interaction involving atoms i and j is the ratio $D_{ij}/(r_{vdW,i}+r_{vdW,j})$ where D_{ij} is the experimental distance between i and j and rvdW,i and rvdW,j are the van-der-Waals radii of i and j (Bondi, A. van der Waals Volumes and Radii. *J. Phys. Chem.* **1964**, *68*, 441-451). If the electron donor j is an anionic atom, $r_{vdW,j}$ is substituted by $r_{P,j}$, the Pauling ionic radius of anion atom j (Shannon, R. D. Revised effective ionic radii and systematic studies of interatomic distances in halides and chalcogenides. *Acta Crystallogr. Sect. A* **1976**, *32*, 751-767). The value 206 pm is used here for the antimony van der Waals radius (Mantina, M.; Chamberlin, A. C.; Valero, R.; Cramer, C. J.; Truhlar, D. G. Consistent van der Waals Radii for the Whole Main Group. *J. Phys. Chem. A* **2009**, *113*, 5806–5812). N_C is a useful indicator because it allows for a more rigorous comparison of distances between different interacting atoms than absolute values of separations.

(31) Edwards, A. J. *J. Chem. Soc. A* **1970**, 2751-2753.

(32) Metrangolo, P.; Panzeri, W.; Recupero, F.; Resnati, G. ^{19}F NMR Study of the Halogen Bonding Between Haloperfluorocarbons and Heteroatom containing Hydrocarbons. *J. Fluorine Chem.* **2002**, *114*, 27-33.

(33) Baldrighi, M.; Cavallo, G.; Chierotti, M. R.; Gobetto, R.; Metrangolo, P.; Pilati, T.; Resnati, G.; Terraneo, G. Halogen bonding and pharmaceutical cocrystals: The case of a widely used preservative. *Mol. Pharmaceutics* **2013**, *10*, 1760-1772.

(34) Messina, T.; Metrangolo, P.; Panzeri, W.; Ragg, E.; Resnati, G. Perfluorocarbon-Hydrocarbon Self-Assembly. Part 3. Liquid Phase Interaction between Perfluoroalkyl Halides and Heteroatom Containing Hydrocarbons. *Tetrahedron Lett.* **1998**, *39*, 9069-9072.

(35) Szell, P. M. J.; Bryce, D. L. ^{35}Cl Solid-State NMR and Computational Study oh Chlorine Halogen Bond Donors in Single-Component Crystalline Chlorinitriles. *J. Phys Chem. C.* **2016**, 120, 11121-11130.

(36) Szell, P. M. J.; Grebert, L.; Bryce, D. L. Rapid Identification of Halogen Bonds in Co-Crystalline Powders via I-127 Nuclear Quadrupole Resonance Spectroscopy. *Angew. Chem.* **2019**, *131*, 13613-13619.

(37) Xu, Y.; Huang, J.; Gabidullin, B.; Bryce, D. L. A rare example of a phosphine as a halogen bond Acceptor. *Chem. Commun.* **2018**, *54*, 11041-11043.

(38) Xu, Y.; Gabidullin, B.; Bryce, D. L. Characterization of Halogen Bonds. *J. Phys. Chem. A.* **2019**, *123*, 6194-6209.

(39) Kumar, V.; Leroy, C.; Bryce, L. D.; Halide Ion Recognition via Chalcogen Bonding in the Solid State and in Solution. *CrystEngComm*. **2018**, *20*, 6406-6411.

(40) Lommerse, J. P. M.; Stone, A. J.; Taylor, R.; Allen, F. H. The Nature and Geometry of Intermolecular Interactions between Halogens and Oxygen or Nitrogen. *J. Am. Chem. Soc.* **1996**, *118*, 3108-3116.

(41) Grabowski,S. J.; Alkorta, I.; Elguero, J. Complexes between Dihydrogen and Amine, Phosphine, and Arsine Derivatives. Hydrogen Bond versus Pnictogen Interaction. *J. Phys. Chem. A* **2013**, *117*, 3243−3251.

(42) Trujillo, C.; Sánchez-Sanz, G.; Alkorta, I.; Elguero, J. Halogen, chalcogen and pnictogen interactions in $(XNO_2)_2$ homodimers (X = F, Cl, Br, I). *New J. Chem.* **2015**, *39*, 6791-6802.

(43) Dewan, J. C.; Edwards, A. J.; Guerchais, J. E.; Petillon, F. Fluoride Crystal Structures. Part XXVJ Trifluorobis(4-methoxypyridine *N*-oxide)antimony(III) Hydrate. *J. Chem. Soc., Dalton Trans.* **1975**, 2295-2297.

(44) Benjamin, S. L.; Burt, J.; Levason, W.; Reid, G.; Webster, M. Synthesis and structures of antimony trifluoride complexes with N-heterocyclic ligands. *J. Fluorine Chem.* **2012**, *135*, 108-113,

(45) Sheldrick, G. M. SADABS; University of Göttingen: Germany, 2012.

(46) Sheldrick, G. M. A Short History of SHELX. *Acta Crystallogr., Sect. A: Found. Crystallogr.* **2008**, *A64*, 112−122.

(47) Sheldrick, G. M. Crystal Structure Refinement with SHELXL. *Acta Crystallogr., Sect. C: Struct. Chem.* **2015**, 71, 3−8.

(48) Macrae, C. F.; Bruno, I. J.; Chisholm, J. A.; Edgington, P. R.; McCabe, P.; Pidcock, E.; Rodriguez-Monge, L.; Taylor, R.; Van De Streek, J.; Wood, P. A. Mercury CSD 2.0 - New Features for the Visualization and Investigation of Crystal Structures. *J. Appl. Crystallogr.* **2008**, *41*, 466−470.

(49) Frisch, M. J.; Trucks, G. W.; Schlegel, H. B.; Scuseria, G. E.; Robb, M. A.; Cheeseman, J. R.; Scalmani, G.; Barone, V.; Petersson, G. A.; Nakatsuji, H.; Li, X.; Caricato, M.; Marenich, A. V.; Bloino, J.; Janesko, B. G.; Gomperts, R.; Mennucci, B.; Hratchian, H. P.; Ortiz, J. V.; Izmaylov, A. F.; Sonnenberg, J. L.; Williams-Young, D.; Ding, F.; Lipparini, F.; Egidi, F.; Goings, J.; Peng, B.; Petrone, A.; Henderson, T.; Ranasinghe, D.; Zakrzewski, V. G.; Gao, J.; Rega, N.; Zheng, G.; Liang, W.; Hada, M.; Ehara, M.; Toyota, K.; Fukuda, R.; Hasegawa, J.; Ishida, M.; Nakajima, T.; Honda, Y.; Kitao, O.; Nakai, H.; Vreven, T.; Throssell, K.; Montgomery, J. A., Jr.; Peralta, J. E.; Ogliaro, F.; Bearpark, M. J.; Heyd, J. J.; Brothers, E. N.; Kudin, K. N.; Staroverov, V. N.; Keith, T. A.; Kobayashi, R.; Normand, J.; Raghavachari, K.; Rendell, A. P.; Burant, J. C.; Iyengar, S. S.; Tomasi, J.; Cossi, M.; Millam, J. M.; Klene, M.; Adamo, C.; Cammi, R.; Ochterski, J. W.; Martin, R. L.; Morokuma, K.; Farkas, O.; Foresman, J. B.; Fox, D. J. Gaussian, Inc., Wallingford CT, 2016. Gaussian 03. *Revis. B.04*.

(50) Metz, B.; Stoll, H.; Dolg, M. Small-Core Multiconfiguration-Dirac-Hartree-Fock-Adjusted Pseudopotentials for Post-d Main Group Elements: Application to PbH and PbO. *J. Chem. Phys.* **2000**, *113*, 2563-2569.

(51) Peterson, K. A. Systematically Convergent Basis Sets with Relativistic Pseudopotentials. I. Correlation Consistent Basis Sets for the Post-d Group 13-15 Elements. *J. Chem. Phys.* **2003**, *119*, 11099-11112.

(52) Peterson, K. A.; Puzzarini, C. Systematically Convergent Basis Sets for Transition Metals. II. Pseudopotential-Based Correlation Consistent Basis Sets for the Group 11 (Cu, Ag, Au) and 12 (Zn, Cd, Hg) Elements. *Theor. Chem. Acc.* **2005**, *114*, 283-296.

(53) Peterson, K. A.; Shepler, B. C.; Figgen, D.; Stoll, H. On the Spectroscopic and Thermochemical Properties of ClO, BrO, IO, and Their Anions. *J. Phys. Chem. A* **2006**, *110*, 13877-13883.

(54) Woon, D. E.; Dunning, T. H. Gaussian Basis Sets for Use in Correlated Molecular Calculations. III. The Atoms Aluminum through Argon. *J. Chem. Phys.* **1993**, *98*, 1358-1371.

(55) Dunning, T. H. Gaussian Basis Sets for Use in Correlated Molecular Calculations. I. The Atoms Boron through Neon and Hydrogen. *J. Chem. Phys.* **1989**, *90*, 1007-1023.

(56) E. D. Glendening, A. E. Reed, J. E. Carpenter, and F. Weinhold. NBO Version 3.1.